SARTORIUS

Application Note

October, 2025

Keywords or phrases:
Flexsafe STR®, Biostat®, Univessel® SU 10 L, Ambr® 250, single-use bioreactor, cell culture, characterization, scaling, CFD, hydrodynamics, biopharma manufacturing, process transfer

Characterizing Mixing, Bubble Distribution, and Oxygen Transfer in Flexsafe STR®, Univessel® SU 10 L, and Ambr® 250 Single-Use Bioreactors for Scalable Process Development

Karl Scheibenbogen[1], Marco Leupold[1], Abhinav Hazarika[1], Vincent Bernemann[2], Michael Schlüter[2]

[1] Sartorius Stedim Biotech GmbH, August-Spindler-Strasse 11, 37079 Goettingen, Germany
[2] Institute of Multiphase Flows, Hamburg University of Technology, Hamburg, Germany

Correspondence
Email: karl.scheibenbogen@sartorius.com

Abstract

System characterization data for single-use cell culture bioreactors play an important role in successfully transferring biopharmaceutical processes from development to manufacturing scales. Within the Sartorius upstream portfolio, a risk-based strategy using a scale-conversion tool has already demonstrated success in addressing key scaling challenges such as gas transfer and agitation rates.

To confirm a simple scale conversion based on geometrical similarity, visual methods assessing mixing and spatial bubble distribution have been added. These methods are correlated against sensor-based measurements to determine power input and oxygen mass transfer. Hydrodynamic parameters gained from bioreactor simulations complete this work to provide a full scaling picture.

In this application note, we identify a promising approach to focusing on stirrer tip speed, volumetric gassing rates, and maintaining shear limits by power input. Deviations and exceptions discerned have been described, and appropriate mitigation proposed.

For more information, visit
sartorius.com

Introduction

Single-use stirred-tank bioreactors are increasingly used in biopharmaceutical manufacturing owing to their flexibility, reduced risk of cross-contamination, and lower capital investment compared to traditional stainless-steel systems. However, their successful implementation—especially when transitioning from laboratory to production—requires thorough bioreactor characterization to enable efficient process transfer.

Standard sensor technologies can be used to assess conditions at specific locations that represent the overall bioreactor environment. This approach enables the evaluation of traditional point-scaling parameters like volumetric power input (P/V), gas mass transfer, and mixing. Matching the design space between scales is important to meeting quality-by-design requirements and is typically simplified by similar system geometry. In addition, risk-based scaling predictions—which consider multiple parameters across multiple scales simultaneously[1]—have been successfully implemented and confirmed for the transfer of a fed-batch CHO culture from 250 mL development to 2,000 L manufacturing scale.[2] Transparent replicas of the vessels also provide valuable visual insights that complement these analytical methods.

This work outlines optical procedures to better characterize mixing in single-use bioreactors through color change methods and spatial bubble distribution, assessed by stirrer energy dissipation using images taken by a high-speed camera. The volumetric mass transfer coefficients (k_La) were determined to validate the bioreactor replicas' performance and establish cross-references between systems. Evaluation and comparison of these key parameters supported robust scaling and the generation of reliable computational fluid dynamics (CFD) models to assess additional factors such as shear and liquid hydrodynamics. Together, these insights facilitate regulatory compliance and cost efficiency, ultimately contributing to the successful commercialization of biopharmaceutical products across scales from 250 mL to 2,000 L.

Materials and Methods

Based on the technical drawings of the Biostat STR® bag holder and the Flexsafe STR® standard designs, acrylic twins were constructed to replicate the original system as closely as possible. Core elements of the Flexsafe STR® Bag were represented by the inbuilt shaft with two stirrer blades attached and a sparger combination with a circular arrangement of 0.8 mm bore-size orifices (ring sparger) and an inner area with 0.15 mm holes (micro sparger) centered below. The final assembly was installed in a supporting structure and fitted with the original shaft, impellers, spargers, and tube sets. An LED panel was installed behind the reactor to provide uniform lighting for optical investigations.

Benchmark data on the volumetric mass transfer coefficient (k_La) were measured in aqueous phosphate-buffered saline (PBS) solution and compared to data evaluated by Sartorius within original Flexsafe STR® Bags using the dynamic method according to the DECHEMA Guidelines[3] at 37 °C. A Biostat STR® II control tower unit was used to monitor stirrer speed, gassing, and dissolved oxygen (DO) concentration, which was measured using two fast-responding optical oxygen probes (WTW FDO®925 and Hamilton OXYFERM® XL). To determine the mass transfer coefficient during DO recordings, the positioning of probes at the top area and lateral sensor belt within the Biostat STR® 2,000 L replica did not reveal any divergence. Consequently, in this work, we only refer to data obtained at the sensor window level.

Ambr® 250 High Throughput and Univessel® SU 10 L vessels were originally designed with transparent materials, enabling visual insights. Images of spatial bubble distribution and mixing videos were recorded by a Nikon D7500 camera. Mixing experiments were carried out by the decolorization of the pH-sensitive tracer phenolphthalein in deionized water at room temperature by adding acid from the top (color change method) and compared to historically generated data using standard DECHEMA guidelines. Further details on the methodology for mixing and spatial bubble distribution, along with some example videos, are available in Scheibenbogen et al.[4] Torque measurements were carried out on the bioreactor shaft using a DRVL sensor and a GMV2 switch box (ETH Messtechnik) according to the DECHEMA recommendations. A similar setup was described by SC Kaiser et al.[5] CFD studies were conducted using M-Star CFD® software (Dotmatics) based on the Lattice-Boltzmann method.

Result

Mixing Time

The mixing performance of all system sizes has previously been evaluated using the iodometry method[3] within their original containers. For Flexsafe STR® Bags, additional windows were cut into the top bag area to improve insights into the bioreactor volume. Although only the small Ambr® 250 vessel is considered a true baffled tank, the dimensionless mixing time Θ, which is the product of determined mixing time ϑ_m (s) and the stirrer rotation speed n (s^{-1}) $\Theta = \vartheta_m \times n$, is almost constant across Sartorius' single-use bioreactor portfolio, independent of tip speed range and system size, as shown in Figure 1.

Figure 1: *Similar Mixing Time Constants Θ vs. Scales at Different Tip Speeds*

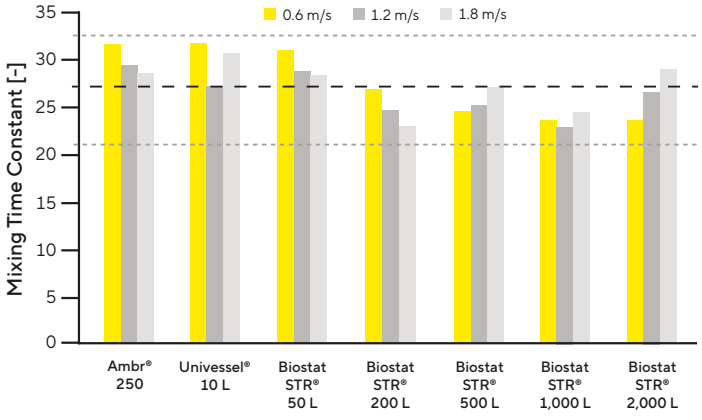

Note. Experiments were conducted at maximum working volume with a two-segment impeller configuration without gassing. Dashed lines indicate two standard deviations

Figure 2: *Images of Decolorization Progress in the Biostat STR® 2,000 L After 23 Seconds With Two-Segment Impellers (Left) and With More Dye Residues Below the Rushton Stirrer (Right)*

The transparent replicas of the Biostat STR® provided improved visibility and were used to assess global and local mixing using the color change method, which works by applying a pH shift. Digital images and average gray value analysis allow a more automated determination of the mixing time required to reach 95% homogeneity (global mixing, $\vartheta_{m,global}$).

For the 200 L and 2,000 L replicas, $\vartheta_{m,global}$ aligns closely with the lower deviation observed in Figure 1 and remains within an acceptable range. However, visual assessment of local mixing — defined as the point when all visible color disappears — showed slightly longer times than those determined by iodometry, especially at larger scales where this discrepancy becomes more pronounced.

The impact of stirrer configurations tested resulted in inconsistent findings, where a Rushton impeller at the lower position improved performance by radial turbulence in the Biostat STR® 200 L. However, the opposite effect was seen at larger scales. Even though the power input increases (e.g., Biostat STR® 2,000 L at 1.8 m/s tip speed from 30 to 47 W/m³), the strong down-pumping activity of segment impellers prevented slow decolorization close to the sparger element (see the comparison in Figure 2). The local mixing time extended from 32 seconds axial flow to 40 seconds with the Rushton impeller, an unexpected result which could suggest a weakened baffling effect at larger scales. Due to the improved visibility afforded by transparent tanks, the prolonged local mixing was unsurprisingly underestimated. However, as illustrated in the following example, the gradient formation can be ruled out if moderate stirrer speeds are applied.

Within the worst-case scenario for the Biostat STR® 2,000 L, a cold bolus addition via headspace was simulated by applying a similar decolorization method to evaluate the maximum temperature gradient. Mixing performance at 1.2 m/s was sufficient to allow just slight deviations between the top compartment and the probe position of less than 0.3 °C.[6]

Figure 3: *Images Showing the Last Areas Mixed in the Biostat STR® 200 L With 0.3 m/s Tip Speed After 23 Seconds Without Gassing (Left), Plus 0.05 vvm Aeration (Right)*

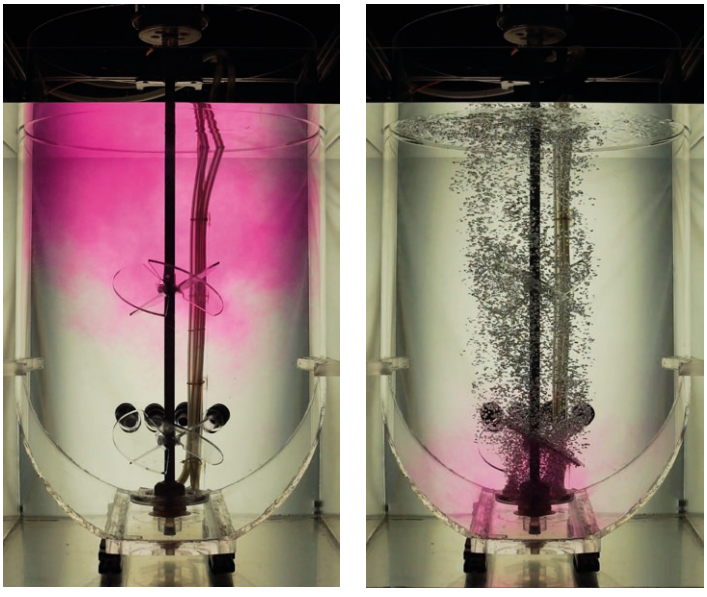

Blending time is influenced not only by stirring-related energy dissipation but also by active gassing. Gassing rates starting at 0.02 vvm reduce decolorization times by up to 25% compared to non-gassed values, particularly at low tip speeds (e.g., Biostat STR® 2,000 L at 0.3 m/s from 200 seconds to 52 seconds with 0.05 vvm ring sparging). Even at moderate impeller speeds, if a homogeneous bubble flow pattern has not yet fully developed, the resulting turbulence can exceed the performance observed under non-gassed conditions (Biostat STR® 2,000 L at 1.2 m/s Rushton and 0.025 vvm micro-sparging, with 25 seconds the smallest value determined at this scale). This effect may relate to effective buoyancy driven flows generated and will be addressed in the following chapter on spatial bubble distribution.

However, special care is needed if gassing rates below 0.02 vvm coincide with low stirring speeds: within the 200 L replica at 0.3 m/s tip speed and 0.015 vvm, it took 60 seconds instead of 36 seconds (with Rushton impeller and no gassing) to clear all red color. Applying the same conditions to the 2,000 L replica — but increasing stirrer tip speed to 0.6 m/s mixing time — increases mixing time from 85 seconds to 130 seconds. This counter-effect is not visible (or is far less significant) with two-segment impellers.

Notably, the local areas showing the slowest decolorization change from the top region (in non-gassed conditions) to the lower zones close to lateral sensor belt (Figure 3), which could impact sensor response time if liquid feed addition is carried out via headspace. However, in all experiments done, no permanent dead zones were identified. As the mixing times of the Ambr® 250 vessels are already in the range of 5 seconds and below at moderate tip speeds (> 0.58 m/s), the impact of gassing is negligible. Minor differences related to the injection area (top vs. bottom) are described by Anand et al[7], who compared the dye blending method with CFD data. For scalability reasons, we continued to focus on the two-segment combination pump-down direction, as there are no segment + Rushton configurations available with Ambr® 250 and Univessel® 10 L vessels.

Single-Phase Computational Fluid Dynamics Simulations

We loaded geometry files for Ambr® 250 High Throughput, Univessel® SU 10 L, and Biostat STR® 50 L tanks, and evaluated the impact of tip speed on liquid velocity at moderate energy dissipations and maximum working volumes (media: water at 20 °C). To validate the single-phase model and grid density applied, simulated mixing times were compared to the previously determined experimental values.

Figure 4: ***(A)*** *Quartile Chart Blending Results in a Biostat STR® 50 L at 150 rpm.* ***(B)*** *Evaluation of Local Mixing by Pixel Analysis Showing Decreasing Quality at Lower Areas and Close to Dip Tubes.* ***(C)*** *Real Color Distribution Using Bromothymol Blue Method (Close to 95% Homogenization).* ***(D)*** *Simulation Plot at a Similar State*

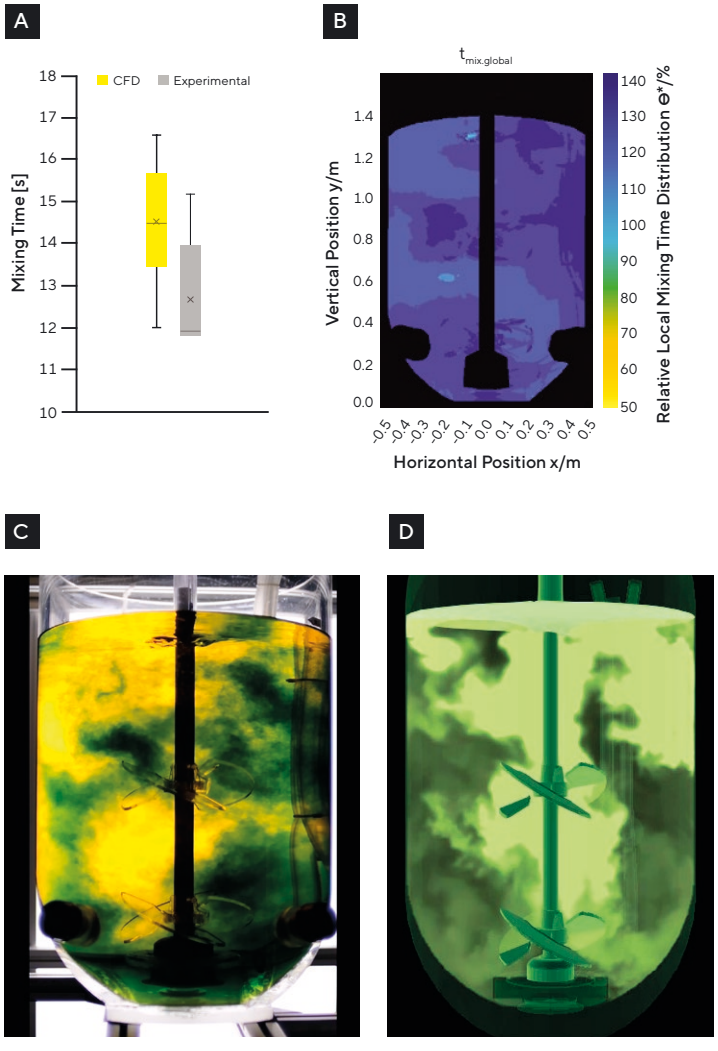

The results show good agreement when filling volumes ranged between 66% and 75% of the maximum. For example, 33 L within a Biostat STR® 50 L at 150 rpm yielded an average simulated mixing time of 7.6 seconds, matching experimental expectations. However, when simulations were run at maximum working volumes, CFD studies revealed longer mixing times than expected, exceeding values of 40 for Θ, and thus the upper standard deviation in Figure 1.

This trend was valid for all tested products. Therefore, the initial parameters (point of tracer addition at the free surface, addition time, and geometry of tracer body) were varied to examine the impact on the outcome more closely. Additionally, a novel color change method proposed by Fitschen et al[8] using bromothymol blue was applied to better represent local mixing effects. For the 50 L and 150 rpm use case, the scores of several run simulations and experiments are shown in a quartile box chart (Figure 4A).

A wide spread in CFD blending times, from 12 seconds to almost 17 seconds, demonstrates that slight changes in tracer injection point at the top free surface can substantially impact outcomes. As is known among computational scientists, maintaining exact boundary conditions means time-dependent computations are not necessarily 100% reproducible.[9]

The average global mixing time observed in the experiments was shorter than both the relative local mixing distribution (Figure 4B) and the visual video analysis, which indicated a central value of about 12 seconds and deviations up to 15 seconds, even when the injection point was unchanged. Therefore, although there is a noticeable overlap between the two result sets, accurately determining the mixing time is less straightforward than initially assumed.

The remaining differences between the simulation and the experiment require further research and cannot be answered conclusively in this paper. However, the overlapping results, similar evolution of marker concentrations (Figure 4C and D), and similar CFD values (6.3 seconds for 400 rpm vs. 5.7 seconds at 450 rpm) published for Ambr® 250,[7] we consider the CFD results validated with regards to scaling purposes.

As shown by Šrom et al,[10] the addition of sufficient poloxamers to cell culture media could mitigate the impact of bubble bursts on cell viability. Consequently, above moderate stirring speeds, liquid velocity differentials and mechanical energy dissipation become the dominant contributors to growth inhibition by shear load. To gain insights into fluid dynamics across scales, a single-phase CFD assessment was applied. Figure 5 visualizes the liquid velocity magnitude and corresponding volumetric power input at maximum working volume.

The numerically predicted velocity distribution confirmed similar downward flow patterns across scales, driven by equal segment impeller configurations. However, areas of higher flow dynamics close to the stirrer blades are much more pronounced in the larger bioreactors. In contrast, considering the eddy dissipation rate (EDR), the rainbow color maps were largely similar (mean time averaged EDR was ~ 35 mW/kg), although a more rapid decrease of eddies in the upper fluid volume of the Ambr® 250 was observed (Figure 6).

Figure 5: *Comparison of Instantaneous Flow Across Scales*

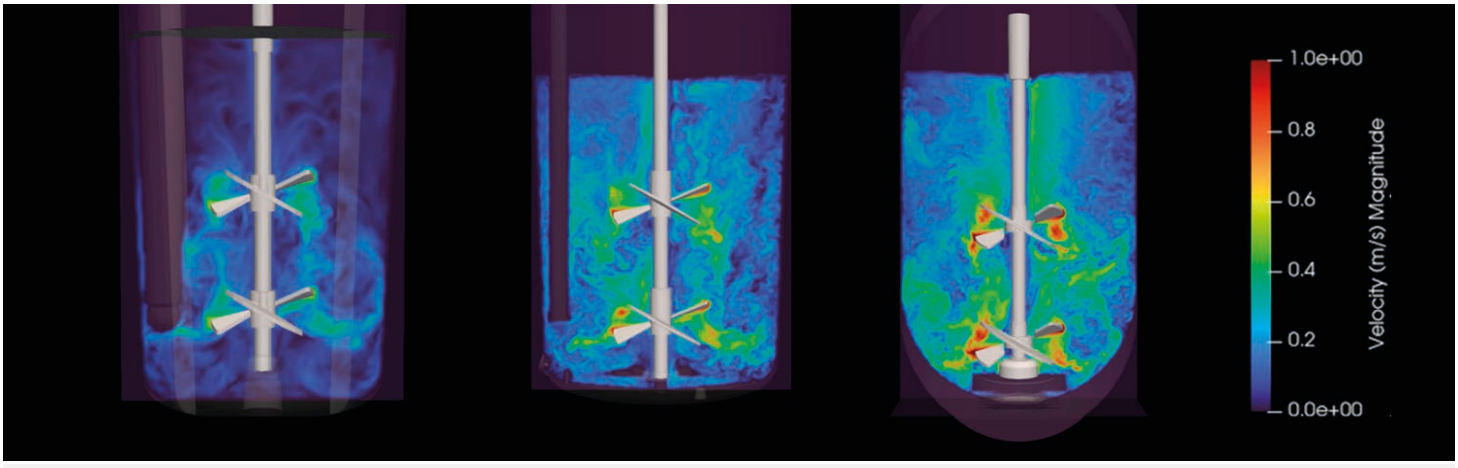

Ambr® 250	Univessel® SU	Biostat STR®
Volume: 250 mL	Volume: 10 L	Volume: 50 L
Agitation: 400 rpm	Agitation: 200 rpm	Agitation: 150 rpm
P/V: 33 W/m³	P/V: 37 W/m³	P/V: 20 W/m³

Figure 6: *Eddy Dissipation in the Ambr® 250 (Left), Univessel® SU 10 L (Center), Biostat STR® 50 L (Right)*

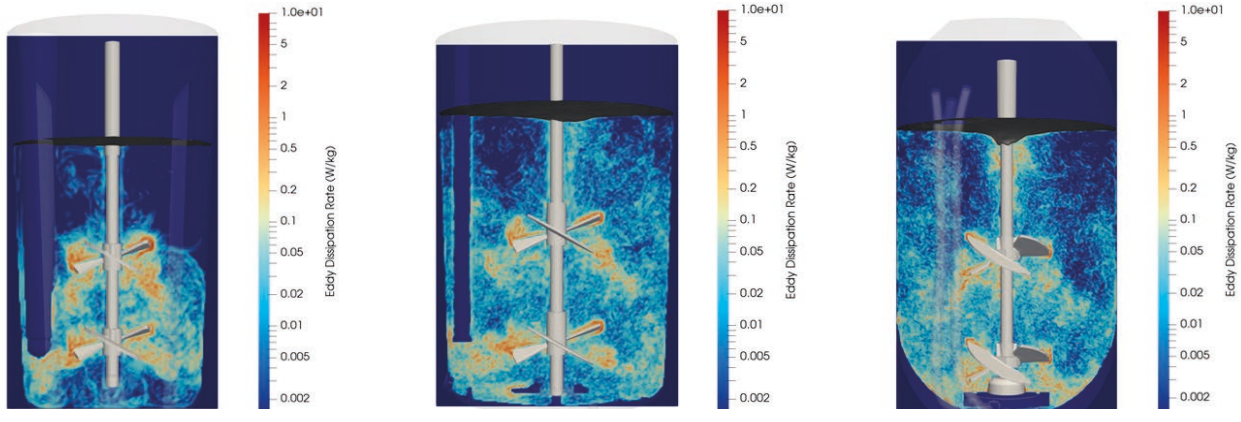

Note. Conditions are the same as in Figure 5

When both velocity and dissipation results are analyzed relative to tip speed, the maximum velocity achieved across all three scales is comparable, as expected. Although we observed a faster velocity decay across the Ambr® 250 volume, indicated by a lower slope with respect to the mean liquid velocity (Figure 7A), the baffled Ambr® 250 vessel causes a higher volumetric power input (P/V) and thus a larger overall energy dissipation rate at the same tip speed (Figure 7B).

Figure 7: *Comparison of **(A)** Mean Liquid Velocity and Eddy Dissipation Rate vs. **(B)** Stirrer Tip Speed Across Three Scales*

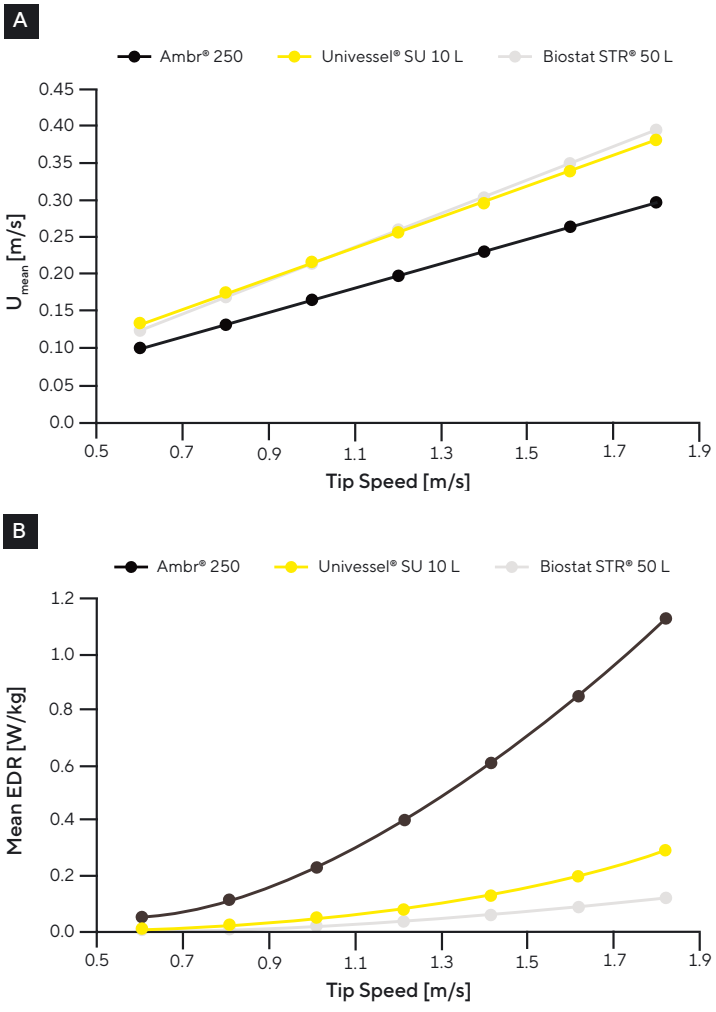

Note. Values interpolated

The maximum effective hydrodynamic shear a cell can experience is impacted by the areas of highest energy dissipation and the likelihood of a cell encountering high-shear zones. The flow field profiles of high dynamics are found close to the impeller tips; thus, knowing the max EDR at different stirrer speeds enables the calculation of the potential highest shear stress (Figure 8).

Figure 8: *Maximum Hydrodynamic Shear Stress for Ambr® 250, Univessel® SU 10 L, and Biostat STR® 50 L at Max. Working Volume, Developed by Stirring Activity*

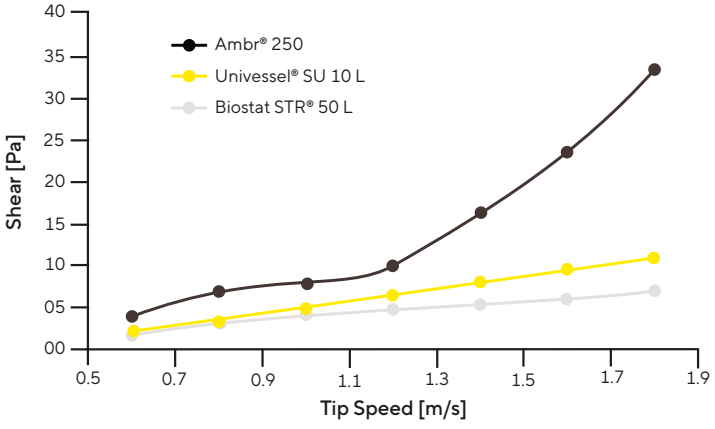

For bioreactor volumes of 10 L and above, the expected shear stress remains below the detrimental limits (20–35 Pa).[11] However, the dynamic environment of Ambr® 250 vessels increases the risk of potential cell damage. While scaling via power input would account for this shear increase, other factors—such as constant hydrodynamics, gas distribution, and mass transfer—could be given priority (as discussed in the following chapters). To find the right balance, it may be advisable to limit impeller frequency in the Ambr® 250 to remain within acceptable mechanical stress levels, while tolerating lower P/V values at larger scales where higher tip speeds can still be applied. CFD modeling for volumes above 50 L is in preparation, and further results, including details about models applied, will be published separately.

Spatial Bubble Distribution Across Reactor Volumes

Gas bubbles distributed throughout the reactor volume impact the flow dynamics, mass transfer, and foam formation, and are often assumed to be similar during process transfer between scales. However, as shown in Figure 3, at low mechanical power inputs, the formation of a bubble plume above sparger orifices can be observed. As stirring energy increases, an improved spatial distribution is expected, with a transition from heterogeneous to homogeneous gas distribution. This can be confirmed for the Sartorius bioreactor portfolio from 250 mL to 200 L; Figure 9 shows the spatial bubble distribution within the 50 L replica as a representative system (see also Anand et al[7] on spatial variation of mass transfer within simulated local Ambr® 250 volume).

The bubble field inserted by micro-sparging expands from the shaft axis toward the bioreactor wall to a final uniform distribution with increasing tip speed.

The ring-sparger clearly releases larger bubbles into the system, but follows a similar flow pattern. In combination with a Rushton impeller, bubbles leaving the ring sparger reach similar sizes to those generated by the micro-sparger, and even slightly improved oxygen mass transfer at maximum stirrer speed in the 50 L bioreactor. However, this occurs at the cost of nearly doubling the energy input compared to two-segment impellers.

At scales above 500 L, the lack of baffles becomes more pronounced, and the bubble flow pattern differs from the 50 L experience. At tip speeds below 1 m/s, a decentered bubble column may rotate through the bioreactor volume. The bubbles rising off the shaft axis generate additional flow dynamics (circular loop in combination with impeller down-pumping), driven by buoyancy forces. These forces promote mixing (as mentioned above) and spark better oxygen mass transfer, as expected.

Figure 9: *Images Showing the Transition From Heterogeneous to Homogeneous Gas Distribution in the Biostat STR® 50 L. Two-Segment Impeller With 0.1 vvm Gassing Rate at 0.6 m/s (Left), 1.2 m/s (Center) and 1.8 m/s Tip Speed (Right)*

Figure 10: *Images Showing Transition From Heterogeneous to Homogeneous Gas Distribution in the Biostat STR® 2,000 L. 0.3 m/s Tip Speed With 0.05 vvm Aeration (Left), 1.2 m/s Tip Speed With 0.025 vvm (Center), and 1.8 m/s Tip Speed With 0.1 vvm*

As tip speed increases to 1 – 1.2 m/s, smaller bubbles are increasingly pushed towards the center by growing centrifugal forces. This results in a more obvious accumulation of the gas phase along the bioreactor shaft compared to smaller scales. However, further increases in tip speeds cause bubble flow to recover to a more homogenous distribution. Figure 10 shows threshold images from the Biostat STR® 2,000 L for all conditions mentioned.

The concentration of the gas phase along the stirrer shaft is also impacted by the way turbulence is initiated. In the event of a process interruption, gassing should be re-established before moderate stirring activity restarts; otherwise, an unfavorable bubble distribution can cause mass transfer drops of 30% or more. However, further increases to maximum stirring energy cause bubbles to be re-dispersed to the desired homogeneous gas flow, as shown at smaller scales. Despite this, small bubbles still tend to accumulate at the shaft axis. This effect is enhanced when using a Rushton impeller; therefore, combining this stirrer type with micro-sparging is not recommended for effective oxygen mass transfer in Flexsafe STR® systems of 500 L and above.

Buoyancy-driven flow can also impact the overall energy dissipation by mechanical stirring. The volumetric power input is usually determined in ungassed systems, as the expected gas holdup at typical cell culture flow rates is generally negligible. However, the strong upflow of a bubble plume along the shaft can counteract the downflow activity of segment impellers to a measurable extent. Figure 11 illustrates the influence on power input when the ring sparger and micro sparger are operated at maximum gassing rate.

Figure 11: *Increase of Mechanical Power Input at High Gas Flow Rates in the Biostat STR® 1,000 L With Two-Segment Impellers*

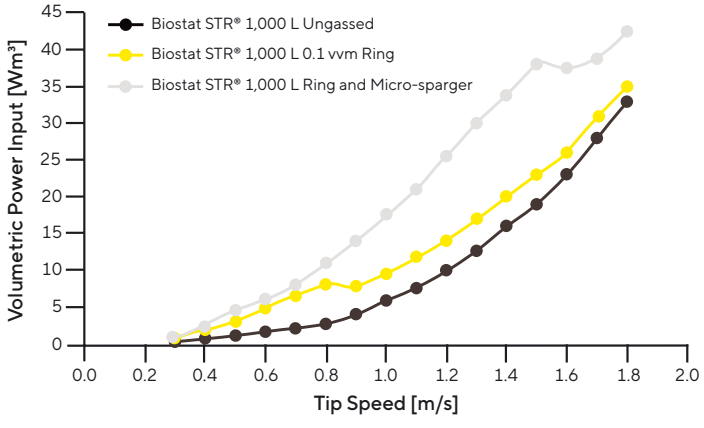

The results obtained by torque measurement support the hypothesis of a transition to homogeneous gas flow at 0.8 m/s tip speed and 0.1 vvm ring-sparger aeration rate, and at 1.5 m/s if 0.1 vvm micro-sparging is added. Just before this point, the calculated P/V is almost doubled by gassing activity. Even at maximum tip speed, volumetric power input remains elevated by approximately 20% when maximum gassing is applied. This effect is clearly diminished when a Rushton impeller is used. It should be noted that this increase is considered exceptional, specific to certain large-scale configurations and very high gassing rates. Under standard conditions, the torque increase remains within the standard deviation of measurement error and can thus be considered negligible.

Oxygen Mass Transfer

As shown in the previous chapter, volumetric power input must be critically evaluated when scaling across bioreactors in the Sartorius portfolio. Although the geometry is very similar, the decreasing impact of fixtures on turbulence creation in larger bioreactors can promote surface vortex formation, requiring unrealistically high stirrer frequencies to match the mechanical energy dissipation observed in the Ambr® 250. Maintaining a constant tip speed is a more robust parameter and is, therefore, used exclusively in mass transfer assessments.

For low oxygen-demanding processes (k_La values below 25 h^{-1}), the spatial bubble distribution generated by stirring energy in combination with the segment + Rushton impeller appears best suited to reflect Ambr® 250 performance (Figure 12).

Figure 12: *Comparison of Mass Transfer vs. Tip Speed in the Ambr® 250 and Various Biostat STR® Sizes With Rushton | Segment Impeller Configuration*

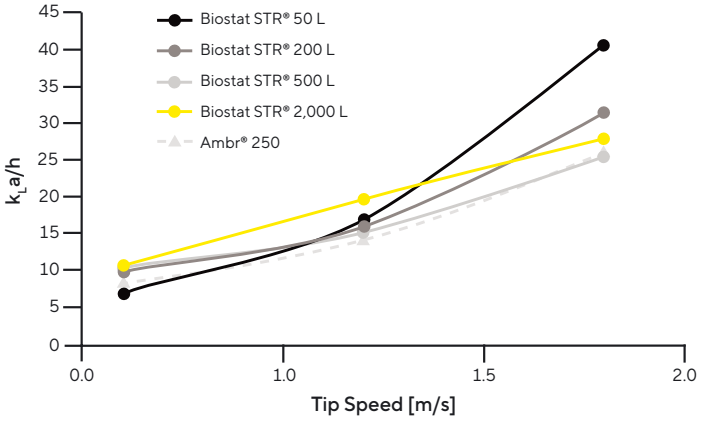

Note. 0.1 vvm gassing rate; ring sparger

At maximum stirring speeds, however, the Biostat STR® 50 L and 200 L equipped with Rushton impellers demonstrate higher oxygen transfer capability compared to larger volumes, and gassing rate may be reduced in this range. With the two-segment impeller configuration, adjustments to the gassing rate would be required over the total stirring speed range, but it is also possible to scale. For highly demanding processes, the micro-sparger would typically be applied to lower the overall gas throughput. The smaller bubbles inserted and longer residence times result in a positive effect on oxygen transfer which is more pronounced at larger volumes.

Figure 13: *Comparison of System Mass Transfer Coefficients at Varying Tip Speeds Across Bioreactor Scales*

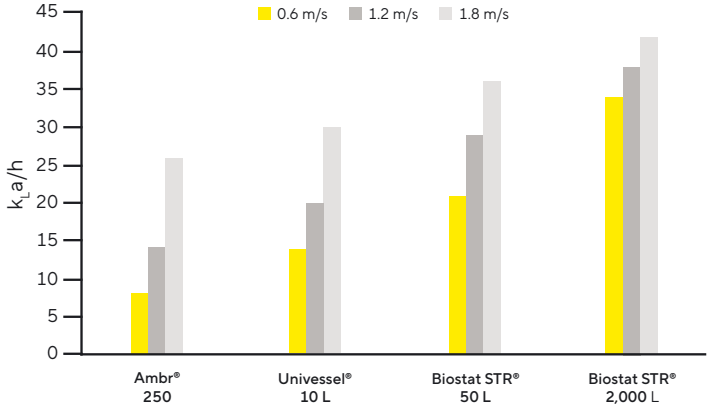

Note. Biostat STR® bioreactors had two-segment impellers and 0.1 vvm gassing rate with micro-sparger. Ambr® 250 had an open pipe sparger

As a result, gassing rates cannot be scaled linearly to maintain comparable performance to the Ambr® 250. A direct comparison of oxygenation capacity across scales can be made by plotting the predicted mass transfer coefficient of one system against that of another.

In Figure 14, the diagonal line would represent a perfect match between Biostat STR® 200 L and the Biostat STR® 1,000 L behavior at 0.1 vvm gassing rate. To compensate for scale-related effects, a lower gassing rate for the Biostat STR® 1,000 L would achieve a similar performance. With increasing tip speed, the performance of the 1,000 L bioreactor slightly drops due to scale-dependent limitations in the vortex-breaking capacity. A further incremental increase in gas flow, beginning at 1.4 m/s tip speed, can equalize even Ambr® 250 open pipe behavior (Figure 15).

Figure 14: *Oxygen Transfer Capability Expressed as Predicted k_La Values in a Micro-Sparging Biostat STR® 200 L at 0.1 vvm vs Biostat STR® 1,000 L at 0.065 vvm from 0.6 – 1.8 m/s Tip Speed*

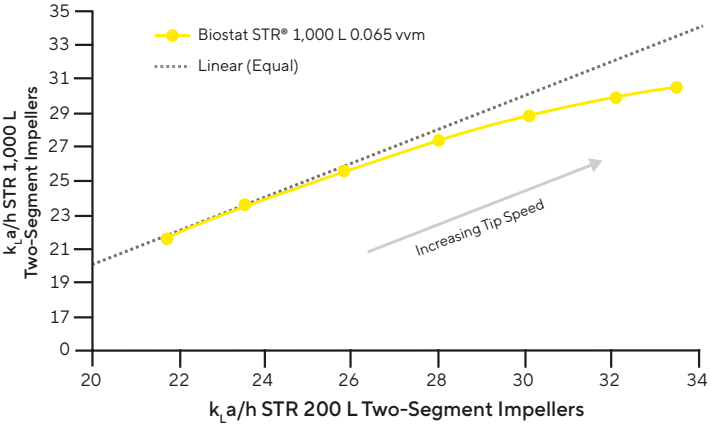

Figure 15 shows that, by reducing initial gassing rates according to bioreactor size, consistent oxygen transfer results can be achieved, remaining within a range of three standard deviations. Starting with an Ambr® 250 k_La of around 17/h (corresponding to 1.4 m/s tip speed), gassing rates in larger scales were increased in 0.01 vvm increments for every additional 0.2 m/s tip speed. For example, the Biostat STR® 200 L started with a constant rate of 0.03 vvm from 0.6 m/s to 1.2 m/s stirrer speed and finished with 0.06 vvm at 1.8 m/s. Using this simple gassing strategy, applicable across all Biostat STR® bioreactors, the oxygen mass transfer of the Ambr® 250 system at a constant 0.1 vvm gassing rate can be matched.

Figure 15: *Predicted oxygen Mass Transfer in Flexsafe STR® Bags With Adapted Gassing Rates in Relation to Ambr® 250 at 0.1* vvm

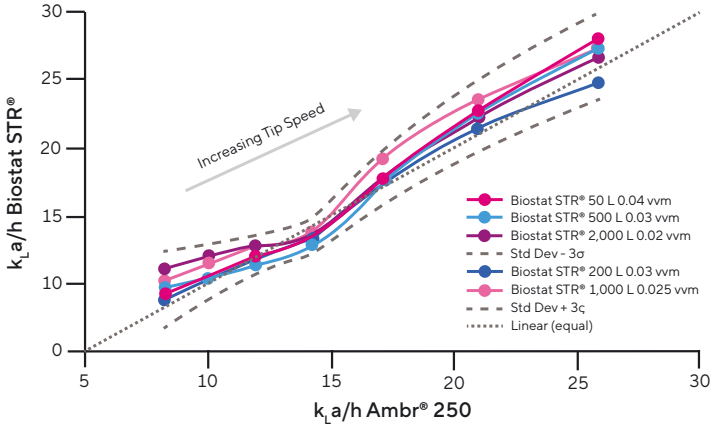

Using the Ambr® 250 vessel as a scale-down model may require higher gassing rates — up to 0.4 vvm — to simulate Biostat STR® behavior. The different gas throughput may influence further parameters like carbon dioxide stripping. However, for intensified high cell density processes, the Ambr® 250 perfusion system is equipped with another sparger type. A scaling strategy for such approaches will be published in a future paper.

Conclusion

By characterizing mass transfer and hydrodynamics with additional visualization methods, we have demonstrated successful scaling and bioprocess optimization across the Sartorius single-use bioreactor portfolio.

Mixing performance confirmed consistent system design across all scales in accordance with mixing time constants, despite some design differences introduced by vessel baffling effects. Although the use of a Rushton impeller generates higher power inputs, the impact on the dye blending behavior can decrease, especially for larger volumes. At gassing rates above 0.02 vvm, bubble-driven fluid flows significantly reduced mixing times, particularly at low agitation rates.

CFD studies confirmed that fluid flow profiles are consistent across bioreactor scales in relation to stirrer tip speeds. Given the higher relative shear stress at maximum tip speeds observed in Ambr® 250 vessel simulation studies, reduced relative agitation rates and corresponding power input could be considered.

The study of spatial bubble distribution also revealed a similar transition to homogeneous gas dispersion with increasing power input. At scales of 500 L and above, the vortex effect becomes more dominant, leading to slightly different flow patterns, even at moderate stirring speeds.
These differences, however, can be compensated for by small adjustments to the gassing rate.

Careful consideration is required if Rushton impeller and micro-sparging are applied to gain better performance; although P/V is increased, the effective oxygen mass transfer is reduced at larger scales because the impact of trailing vortexes by baffles is lacking. In addition, considering only segment impellers, high gas flows can also cause increased volumetric power inputs due to buoyancy-driven flows.

Nevertheless, no drops in performance with respect to oxygen mass transfer were identified. Simple scaling at constant gassing rates from Ambr® 250 open pipe vessels can be implemented using ring spargers and Rushton impellers in Flexsafe STR® bags. For more demanding processes, the use of the micro-sparger enables better transfer rates with maximum kLa values around 40 /h and a consistent two-segment impeller configuration. Notably, the Biostat STR® 50 L Rushton impeller is particularly effective. Lower gassing rates are required to recapitulate the behavior of the Ambr® 250. Future opportunities to implement micro-sparging in Ambr® 250 High Throughput bioreactor format could help align gassing strategies across all scales.

Overall, scaling based on tip speed, rather than P/V, appears to be more effective for unbaffled Biostat STR® systems and yields accurate predictions of mixing and mass transfer behavior. Complete characterization data tables are available using Sartorius scaling tools and related documentation. For more complex scaling requests, including biological performance, we recommend our data analytics consultancy service, which leverages design of experiments and multivariate data analysis tools to ensure process consistency across scales. Please contact your Sartorius representative.

This study underscores the importance of understanding bioreactor dynamics and offers a promising approach to scaling challenges, paving the way for the continued growth and success of single-use technologies in the industry. A summary of all scaling parameters assessed is displayed in Table 1.

Table 1: *Parameters Tested Across the Bioreactor Systems, Main Observations, and the Impact on Scaling*

Scaling Parameters	Characterized Systems	Main Observations	Scaling Impact
Dimensionless mixing time	Ambr® 250, Univessel® SU 10 L, Biostat STR® 50 L – 2,000 L	Similar mixing time constants observed across all scales	Quick reference of stirrer rotation speed vs. mixing time
Mixing and system configuration	Biostat STR® 50 L – 2,000 L	Gassing lowers mixing times, and there is a poor effect of Rushton impellers at large scales	Increased P/V by Rushton impeller does not lead to improved mixing at all scales
Liquid hydrodynamics	Ambr® 250, Univessel® SU 10 L, Biostat STR® 50 L	Similar flow pattern with respect to the stirrer tip speed	Influences the choice of P/V as a scaling factor
Energy dissipation and maximum mechanical shear stress	Ambr® 250, Univessel® SU 10 L, Biostat STR® 50 L	Higher rates in smaller scales at constant tip speed	Consider lower P/V values and gassing rates to match larger-scale conditions
Bubble distribution bioreactor volume	Ambr® 250, Biostat STR® 50 L – 2,000 L	Transition from heterogeneous to homogeneous flows depending on tip speed	Prefer high tip speeds at large scales
Gassed power input	Biostat STR® 1,000 L	Buoyancy flows can increase the stirrer torque measured when two-segment impellers are applied	Carefully consider P/V as scaling factor
Oxygen mass transfer — low demands	Ambr® 250, Univessel® SU 10 L, Biostat STR® 50 L – 2,000 L	Acceptable kLa similarity with respect to tip speed	Consider respective sparger | impeller configurations
Oxygen mass transfer — high demands	Ambr® 250, Biostat STR® 50 L – 2,000 L	Obvious size effect lowers gas requirements at large scales	Adapt gassing rates according to volume and tip speed to generate similarity

References

1. Stacey, A., et al. (2021). A novel, risk-based approach for predicting the optimum set of process and cell culture parameters for scaling upstream bioprocessing. Bioprocessing Journal, 20. https://bioprocessingjournal.com/a-novel-risk-based-approach-for-predicting-the-optimum-set-of-process-and-cell-culture-parameters-for-scaling-upstream-bioprocessing/
2. Ruhl, S., et al. (2020). A rapid, low-risk approach for process transfer of biologics from development to manufacturing. BioProcess International, 18(5). https://www.bioprocessintl.com/sponsored-content/ a-rapid-low-risk-approach-process-transfer-of-biologics-from-development-to-manufacturing-scale
3. DECHEMA. (2020). Recommendations for process engineering characterization of single-use bioreactors and mixing systems by using experimental methods (2nd ed.). https://dechema.de/dechema_media/Downloads/Positionspapiere/Single_Use_BioReactors_2020-p-20006899.pdf
4. Scheibenbogen, K., et al. (2025). Gas-liquid flow, oxygen mass transfer, and mixing characterization of a transparent single-use bioreactor model (Biostat STR® 200). TUUH Open Research Publications. https://tore.tuhh.de/entities/publication/0cfdf39e-eb9f-408e-a71d-b9f97b70932a
5. Kaiser, S. C., et al. (2016). Development of a method for reliable power input measurements in conventional and single-use stirred bioreactors. Engineering in Life Sciences, 16(6), 577–584. https://doi.org/10.1002/elsc.201600096
6. Bernemann, V., et al. (2024). Temperature distribution in a Biostat STR® 2000 single-use reactor using top injection. Internal Publication, Sartorius. DAM ID 270592
7. Anand, A., et al. (2024). An in-silico analysis of hydrodynamics and gas mass transfer characteristics in scale-down models for mammalian cell cultures. Journal of Biotechnology, 388, 96–106. https://doi.org/10.1016/j.jbiotec.2024.04.013
8. Fitschen, J., et al. (2021). Novel evaluation method to determine the local mixing time distribution in stirred tank reactors. Chemical Engineering Science: X, 10, 100098. https://doi.org/10.1016/j.cesx.2021.100098
9. Haringa, C., et al. (2025). Reproducibility of large eddy simulations for mixing in stirred tank reactors. ArXiv Preprint. https://doi.org/10.48550/arXiv.2503.20622
10. Srom, O., et al. (2022). Characterization of hydrodynamic stress in Ambr® 250 bioreactor system and its impact on mammalian cell culture. Biochemical Engineering Journal, 177, 108240. https://doi.org/10.1016/j.bej.2021.108240
11. Neunstoeckling, B., et al. (2015). Determination of the maximum operating range of hydrodynamic stress in mammalian cell culture. Journal of Biotechnology, 194, 100–109. http://dx.doi.org/10.1016/j.jbiotec.2014.12.003

Germany
Sartorius Stedim Biotech GmbH
August-Spindler-Strasse 11
37079 Goettingen
Phone +49 551 308 0

USA
Sartorius Stedim North America Inc.
565 Johnson Avenue
Bohemia, NY 11716
Toll-Free +1 800 368 7178

For more information, visit
sartorius.com

Last modified: 10 | 2025